Published in final edited form as:
Cell Mol Bioeng. 2011 June 1; 4(2): 169–181. doi:10.1007/s12195-010-0136-9.

Endothelial Cell Membrane Sensitivity to Shear Stress is Lipid Domain Dependent

Tristan Tabouillot[1], **Hari S. Muddana**[1], and **Peter J. Butler**[1,2]

[1]Department of Bioengineering, The Pennsylvania State University, 205 Hallowell Building, University Park, PA 16802, USA

[2]Department of Bioengineering, The Pennsylvania State University, 230 Hallowell Building, University Park, PA 16802, USA

Abstract

Blood flow-associated shear stress causes physiological and pathophysiological biochemical processes in endothelial cells that may be initiated by alterations in plasma membrane lipid domains characterized as liquid-ordered (l_o), such as rafts or caveolae, or liquid-disordered (l_d). To test for domain–dependent shear sensitivity, we used time-correlated single photon counting instrumentation to assess the photophysics and dynamics of the domain-selective lipid analogues DiI-C_{12} and DiI-C_{18} in endothelial cells subjected to physiological fluid shear stress. Under static conditions, DiI-C_{12} fluorescence lifetime was less than DiI-C_{18} lifetime and the diffusion coefficient of DiI-C_{12} was greater than the DiI-C_{18} diffusion coefficient, confirming that DiI-C_{12} probes l_d, a more fluid membrane environment, and DiI-C_{18} probes the l_o phase. Domains probed by DiI-C_{12} exhibited an early (10 s) and transient decrease of fluorescence lifetime after the onset of shear while domains probed by DiI-C_{18} exhibited a delayed decrease of fluorescence lifetime that was sustained for the 2 min the cells were subjected to flow. The diffusion coefficient of DiI-C_{18} increased after shear imposition, while that of DiI-C_{12} remained constant. Determination of the number of molecules (N) in the control volume suggested that DiI-C_{12}-labeled domains increased in N immediately after step-shear, while N for DiI-C_{18}-stained membrane transiently decreased. These results demonstrate that membrane microdomains are differentially sensitive to fluid shear stress.

Keywords

Microdomains; DiI; Carbocyanine dye; Fluorescence correlation spectroscopy; Fluorescence lifetime; Molecular brightness; TCSPC

INTRODUCTION

Mechanotransduction is a cellular process by which the sensation of mechanical stimuli is converted to biochemical signaling pathways. Although it is a phenomenon recurrent in animal biology,[54] vascular endothelial cell (EC) mechanotransduction of fluid shear stress has received special attention because of the strong correlation between hemodynamics and the physiology and pathophysiology of blood vessels (reviewed in Davies[17]). Multiple lines of investigation have established that ECs are sensitive to spatial[19,44] and temporal

Address correspondence to Peter J. Butler, Department of Bioengineering, The Pennsylvania State University, 230 Hallowell Building, University Park, PA 16802, USA. pbutler@psu.edu.
Tristan Tabouillot and Hari S. Muddana contributed equally to this work.

gradients[4,11,26] in shear stress and that these changes are mediated by proteins in focal adhesions,[46] the actin cytoskeleton,[28,29] cell–cell junctions[4,27,71] and the glycocalyx.[25,51,56] In addition, endothelial plasma membrane sensitivity to shear stress has been demonstrated by studies measuring lipid mobility,[10] activation of potassium[37,52,53] and stretch-activated calcium[64] channels, phosphorylation of G proteins,[12] conformational changes of G protein coupled receptors (GPCRs), changes in number of caveolae[57,59] and diffusion of the raft-associated protein Lyn.[62]

Many recent studies have now established that the plasma membrane is highly heterogeneous and dynamic. For example, membrane compartments originally designated as detergent-resistant membranes (DRM),[8,9] commonly known as lipid rafts and caveolae, exist in highly transient states,[2] and assist in sorting membrane proteins in order to regulate membrane-based signaling.[63] In addition, interaction of the membrane with the cytoskeleton[42] and glycocalyx[69] play a role in membrane organization by virtue of chemical and steric interaction with lipids and membrane-bound proteins. However, the force distribution between the glycocalyx, membrane, and cytoskeleton, and the role of force in modulating membrane organization is currently unknown.

Since fluid flow near the cell surface may be impeded by the glycocalyx,[14,61] it has been postulated that stress from flow is carried directly from the glycocalyx to the actin cytoskeleton.[70,76] However, the unique force distribution in ECs arising from shear imposition,[5,23] the temporal and spatial variability of consistency of the glycocalyx, and the complex interaction of the glycocalyx with the lipid bilayer lead to the need to test for lipid perturbation by shear stress in intact cell membranes in their natural in situ state, with high spatial and temporal sensitivity. A potential fluorescence method available to probe intact membranes includes fluorescence labeling of GM1-bound cholera toxin B to track lipid raft diffusion in cells. But the ganglioside connection to the cortical cytoskeleton leads to low mobility of fluorescent reporter molecules and subsequent photobleaching of the dye.[3] Lipoid dyes such as dialkylindocarbocyanines (DiI), on the other hand, are more representative of native lipid mobility[33] and present low cytotoxicity. In model membranes, DiI-C_{12} preferentially partitions into liquid phases and DiI-C_{18} into gel phases.[40,66] In cells, DiI-C_{12} predominantly probes fluid (liquid-disordered, l_d) phases while DiI-C_{18} segregates into liquid-ordered (l_o) domains.[34] The photophysics (e.g. fluorescence lifetime, quantum yield) have been well characterized,[55] and because these dyes share identical chromophores and differ only by their chain lengths, they are useful in definitively assigning their unique photophysical properties to different membrane domains. For most other “raft” associated dyes there is no structurally equivalent counter stain to probe non-raft regions.

It is hypothesized in this study that shear stress leads to differential perturbation of membrane microdomains. To obtain data on the transient character of the endothelial plasma membrane domain responses to a step shear,[18] we used time-correlated single photon counting (TCSPC) technology applied to single molecule fluorescence of membrane domain-specific fluorescent dyes. TCSPC can record the arrival times of each fluorescence photon with respect to the laser pulse time with resolution down to 10 s of picoseconds and at repetition rates in the MHz range. Post-processing of accumulated fluorescence photon arrival times provides determination of fluorescence lifetimes and diffusion coefficients, using fluorescence correlation spectroscopy (FCS),[22,49] and number of fluorescent molecules and molecular brightness from moment analysis. TCSPC has been used in cell membrane studies involving FCS, Forster resonance energy transfer (FRET) and fluorescence lifetime imaging (FLIM),[16,21] but only a few studies combining fluorescence lifetime and FCS from the same data have been reported for cells,[6] and there are no published reports on multiparameter TCSPC to elucidate mechanotransduction mechanisms. Here we show that domains defined by DiI-C_{12} and DiI-C_{18} react to shear stress with

differences in diffusion coefficients, fluorescence lifetimes, and number of molecules in the probe volume, results that can be explained by transient, domain-specific shear-induced changes in lipid viscosity, domain organization, and surface topography.

MATERIALS AND METHODS

Flow Setup

The flow loop setup has been thoroughly described previously.[15] Briefly, a step shear stress of 0–10 dyn/cm^2 (with 0.36 s halftime rise) was induced from a pressure gradient delivered through a computer-controlled, six-port modular valve positioner (Hamilton, Reno, NV) connected to four media reservoirs. Inducing flow using equal and opposite pressure changes ensures that there is no pressure change in the chamber itself, and thus prevents coverslip deflection, which could create artifacts in analysis of FCS and other parameters from TCSPC.[68] Physiological conditions were preserved by the use of temperature control in the parallel-plate flow chamber (Focht Chamber System (FCS2)) (Bioptechs, Butler, PA) and the superfusion of 5% CO_2 over the media reservoirs. A differential pressure transducer DP-15 (Validyne Engineering, Northridge, CA) continuously monitored and recorded pressure changes across the flow chamber.

Cell Culture, Methyl-β-cyclodextrin Treatment, and Staining

Bovine aortic endothelial cells (BAECs) (VEC Technologies, Rensselaer, NY) were cultured in MCDB-131 complete medium (450 mL) supplemented with 50 mL FBS (fetal bovine serum), 10 ng/mL EGF (epidermal growth factor), and 1 μg/mL hydrocortisone with addition of 50 μL/mL 100× antibiotic/antimycotic solution, 90 μg/mL heparin, and 0.2 mg/mL ENDO GRO (VEC Technologies, Rensselaer, NY). Cells, passages 5–10, were incubated in this medium at 37 °C with 5% CO_2 and grown to confluence on No. 1 glass coverslips. The medium was changed to phenol red-free Dulbecco's modified Eagle's medium (DMEM) (GIBCO, Carlsbad, CA) with 10% FBS 24 h before the experiment.

For cholesterol depletion experiments, endothelial cells were treated with methyl-β-cyclodextrin (MβCD) following established protocols.[45] In brief, after rinsing with DMEM without serum, the cells were incubated for 30 min in 5 mM methyl-β-cyclodextrin (Sigma-Aldrich, St. Louis, MO) in DMEM without serum and washed three times with serum-free DMEM.

Cell membranes were stained using either 1,1′-dioctadecyl-3,3,3′,3′-tetramethylindocarbocyanine perchlorate (DiI-C_{18}) or 1,1′-didodecyl-3,3,3′,3′-tetramethylindocarbocyanine perchlorate (DiI-C_{12}) (Invitrogen, Eugene, OR). Stock solutions were prepared in ethanol: 1 mM for DiI-C_{18} and 100 mM for DiI-C_{12}. Subsequent dilutions were performed in ethanol and Dulbecco's phosphate-buffered saline (DPBS) with calcium and magnesium to a final concentration of 1 μM. The cells were washed three times in DPBS and then incubated with the staining solution for 3–4 min at 37 °C. The coverslips with cells were washed again five times in DPBS and assembled in the flow chamber in phenol-red free DMEM with 10% FBS.

GUV Preparation

Giant unilamellar vesicles (GUVs) were formed using a modified electroformation technique[20]: an oscillating electric field created between two transparent ITO-coated coverslips, used as electrodes, caused the electroformation of vesicles. Briefly, a lipid mixture comprised of lipid and chloroform solvent was dissolved and 2 microliters of the solution was then placed on the surface of one coverslip and blow-dried with argon. After a 30-min vacuum drying period, the mixture was covered with 0.1 M sucrose solution at 55

°C, a small chamber was assembled and the whole apparatus was then placed in a baking oven maintained at a temperature of 55 °C. An alternating current was applied across the wire electrodes for 4–5 h. A LabVIEW-controlled A/D board (National Instruments, Austin, TX, USA) was used to increase voltage from 0 to 1 V in increments of 50 mV at 5 min intervals, followed by a constant voltage of 1.2 V for 3 h. Subsequently, the whole chamber was disconnected from the voltage supply and the vesicles were gradually cooled to room temperature.

Optical Setup

A detailed description of our confocal molecular dynamics microscope (CMDM) was given previously.[32] In brief, the excitation beam from a PicoTRAIN water-cooled 532-nm, 80-MHz, 5.4-ps pulsed laser (High-Q Laser, Hohenems, Austria) entered the side port of an IX-71 microscope (Olympus, Tokyo, Japan) and slightly underfilled (80%) the back aperture of an Olympus 60×/1.2-NA water-immersion objective.[35] Emitted light passed a polarizer positioned at the magic angle, and was focused onto a 50-μm, 0.22-NA optical fiber—acting as confocal pinhole. The signal from the photomultiplier tube went to a preamplifier and the time-correlated single photon counting (TCSPC) board (HFAC-26 and SPC-630, Becker & Hickl, Berlin, Germany). The cells, vesicles, or solution samples were positioned using a high resolution 3-D piezo-electric stage (NanoView, Mad City Labs, Madison, WI) and imaged using a high-sensitivity CCD camera (Sensicam EM, Cooke Corporation, Romulus, MI).

Single-Molecule Fluorescence Spectroscopy

Time-correlated single photon counting technology allows one to record the arrival time of photons with respect to the beginning of the measurement (macrotime) and with respect to the excitation pulse time (microtime). From the microtime, we built histograms from which fluorescence lifetimes were determined. From the macrotime, recorded in first-in first-out (FIFO) mode, we built autocorrelation functions and used FCS to determine the diffusion coefficients. It is also possible to recover the microtime from FIFO data when using a pulsed laser. Consequently, one data file contained all information necessary to determine diffusion coefficients, fluorescence lifetime, brightness, and number of molecules.

Fluorescence lifetime (τ_{fl}) depends on radiative emission rate (k_r) of photons and on non-radiative decay rate (k_{nr}) via local environmental factors such as viscosity, hydration, oxygen concentration, and ionic strength[43] according to $\tau_{fl} = 1/(k_r + k_{nr})$. Time-dependent fluorescence intensity is usually represented by a sum of exponential decays according to Eq. (1):

$$I(t)=\sum_i \alpha_i \exp\left(\frac{-t}{\tau_{fli}}\right) \quad (1)$$

where α_i is the fraction of molecules with fluorescence lifetime τ_{fli}, normalized to unity.

Fluorescence correlation spectroscopy is used to assess the transport properties of a fluorescently-tagged molecule in an observation volume defined by the diffraction limit of the excitation light beam and the confocal properties of the emission pathway. Fluorescent molecules moving into and out of the observation volume induce bursts in fluorescence which can be correlated in time. The resulting autocorrelation curve is fitted for particular expected transport phenomena. For 2-dimensional free-diffusing multiple species, the fitting function is of the form of Eq. (2):

$$G(\tau)=\left(1-T_r+T_r\cdot\exp\left(-\frac{\tau}{\tau T}\right)\right)\cdot\left(\frac{0.5}{N(1-T_r)}\right)\cdot\sum_{i=1}^{n}b_i\left[1+\left(\tau/\tau_{Di}\right)\right]^{-1} \quad (2)$$

where b_i is the relative fraction of species i, τ_{Di} is the diffusion time of species i and N is the average number of fluorescent particle in the observation volume. The first factor in parentheses accounts for triplet-state blinking: T_r is the average fraction from triplet-state and τ_T is its relaxation time.

Experiments were performed using 100-μW excitation power measured at the objective back aperture[77] and the system was calibrated using free diffusing rhodamine 6G dye (R6G) (Invitrogen, Eugene, OR) with known diffusion coefficient and fluorescence lifetime.[78] The resulting observation volume radius was r ~ 443 nm with a structure factor (axial dimension over radial dimension) maintained under 8.

Fluorescence fluctuations recorded from the FIFO data allow us to gather values for the number of molecules (N) in the observation volume. Correction for the photomultiplier tube counting statistics through calculation of the molecular brightness gives more accurate values for N. Moment analysis is a model-independent and computationally-fast approach to count the number of fluorescence molecules in the observation volume. It is based on the computation of the moments of the photon count distribution from the PMT, where the average number of molecules, $\overline{N}$, is given by Eq. (3):

$$\overline{N}=\frac{\gamma\langle k\rangle^2}{\langle\Delta k^2\rangle-\langle k\rangle} \quad (3)$$

where γ is the geometric factor of the volume, $\langle k\rangle$ is the average photon count and $\langle\Delta k^2\rangle$ its variance. Thus, the molecular brightness, ε is:

$$\varepsilon=\langle k\rangle/\overline{N} \quad (4)$$

Lifetime curves were fitted in Fluofit software (PicoQuant, Berlin, Germany) by iterative reconvolution or tail fitting depending on the case studied (see Results). Goodness of fit was assessed from minimization of the χ^2 values and absence of correlation in the residuals. Statistics and autocorrelation fits from FCS data were performed in Origin software (Originlab, Northampton, MA).

Experimental Procedures

Cellular and model membrane studies were performed over multiple days. Laser position with respect to the imaging system was checked and FCS system was calibrated before each experiment. Once the cells were mounted onto the flow chamber, lateral positioning was accomplished using differential interference contrast (DIC) microscopy. Axial positioning of the observation volume on the apical membrane was set by rapid fluorescence count scan and by checking the autocorrelation curves. A custom-written LabVIEW VI (National Instruments, Austin, TX) controlled stage position and recorded the signal from the pressure transducer.

The effect of shear stress on the apical endothelial cell membrane at a position upstream from the nucleus was studied by recording simultaneously changes in lifetime and diffusion

coefficient of the membrane dye for 2 min before shear, 2 min during a 10 dyn/cm^2 shear, and 2 min after discontinuation of shear. Fluorescence data saved during the overall time of experiment were truncated in discrete steps. Autocorrelation functions from FCS data were computed and analyzed for 20-s time increments, and fluorescence fluctuation and lifetime data for both 20 and 5-s time increments. Significant differences were evaluated by computing two-sample, paired t-tests.

RESULTS

DiI Fluorescence Lifetime and Diffusion Reflect Membrane Microviscosity

We first wished to determine if phase-specific differences in dye photophysics were due to chromophore surrounding (indicative of membrane phase) or resulted from effects of alkyl chain length differences on chromophore non-radiative decay rates.

First, we measured fluorescence lifetime of DiIs in solutions of varying viscosities. Effect of local viscosity on dye lifetimes was estimated by varying the content of reagent-grade glycerol from 0 to 70% (v/v) in ethanol solutions (Fig. 1a). Viscosity of each sample was measured separately with a viscometer. Fluorescence lifetimes were obtained by fitting histograms of arrival times with a double exponential using iterative reconvolution, and diffusion coefficients were determined by fitting autocorrelation curves with models for 3-D diffusion. The values of DiI-C_{12} and DiI-C_{18} lifetime increased similarly for viscosity changes from 1 to 185 cp: $\tau_{1cp,C12} = 0.22 \pm 0.002$ ns, $\tau_{1cp,C18} = 0.22 \pm 0.01$ ns and $\tau_{185cp,C12} = 1.32 \pm 0.01$ ns, $\tau_{185cp,C18} = 1.34 \pm 0.02$ ns. We conclude that fluorescence lifetime of DiI depends on local viscosity surrounding the chromophore and is independent of dye chain length. Next, fluorescence lifetime and diffusion coefficients were measured in giant unilamellar vesicles to assess the behavior of DiI-C_{12} and DiI-C_{18} in membranes exhibiting liquid-disordered (l_d) (DOPC) and liquid-ordered (l_o) (DOPC:cholesterol in a 1:1 mol fraction) phases (Table 1). Ten FIFO measurements, taken at room temperature, were recorded for each data set. Fluorescence lifetimes were obtained by fitting histograms of arrival times with a double exponential using iterative reconvolution, and diffusion coefficients were determined by fitting autocorrelation curves with models for 2-D diffusion. In a given membrane phase, lateral mobility was not significantly affected by the hydrocarbon chain length as evidenced by the similarities in diffusion coefficient of DiI-C_{12} and DiI-C_{18} when dyes were incorporated into like phases of either liquid-disordered ($D_{ld} \sim 8 \times 10^{-8}$ cm^2/s) or liquid-ordered phase lipids ($D_{lo} \sim 5 \times 10^{-8}$ cm^2/s). Attempts to record diffusion coefficients in gel phase, using DPPC, resulted in photobleaching of the immobile dyes, consistent with previous reports.[40] Similarly, fluorescence lifetimes depended on membrane phase and not chain length as shown by the fact that the lifetimes for the two dyes were statistically equivalent when incorporated into equivalent phases.

We then assessed fluorescence lifetimes and diffusion coefficients of dyes in the apical membranes of confluent bovine aortic endothelial cells (Table 1). We first note that the fluorescence lifetime of DiI-C_{12} ($\tau = 1.26 \pm 0.02$ ns) was significantly shorter than that of DiI-C_{18} ($\tau = 1.43 \pm 0.05$ ns) in cells incubated in DMEM with FBS suggesting that the dyes probe environments of differing viscosity. Sequestering of cholesterol from membranes using MβCD caused DiI-C_{18} fluorescence lifetime to be significantly reduced but did not affect fluorescence lifetime of DiI-C_{12}, suggesting that cholesterol is responsible for the formation of viscous domains probed by DiI-C_{18}. In addition, cells in PBS had significantly shorter DiI lifetimes than cells in 10% FBS, indicating that serum proteins play a role in cell membrane viscosity.

Together, control studies in solution and model membranes and studies in cells lead us to conclude that differences in DiI-C_{12} and DiI-C_{18} fluorescence lifetimes, observed in cells,

arise from the dyes' differential preference for membrane phases and are not an artifact of having different chain lengths.

Shear Stress Effects on Cell Membranes are Reflected in Changes in DiI Photophysics

Confluent bovine aortic endothelial cells were subjected to a step shear of 10 dyn/cm^2 from fluid flow, and the photophysics and dynamics of DiI-C_{12} and DiI-C_{18} were recorded continuously. The observation volume was a spot on the plasma membrane on the midpoint between the nucleus and cell border on the upstream of the cell.[10] Fluorescence from DiI embedded in the membrane was collected in FIFO mode, allowing extraction of fluorescence fluctuations and lifetime data. The use of a time-correlated single photon counting-based system allowed us to gather simultaneous information at the nanosecond (fluorescence lifetimes) and micro to milliseconds (lateral diffusion) timescales from single molecules. However, the penalty of increased temporal resolution is fewer photons contributing in each time step. Diffusion coefficients, in particular, require more photons to build and fit the autocorrelation function. In addition, the standard error of FCS measurement reaches 20% for 2-species fits, as seen in model membranes.[41] Considering all the above, the shortest time step for shear effects was 20 s for lateral diffusion, and 5 s for fluorescence lifetime. Measurements of DiI-C_{12} were averaged over 8 cells and DiI-C_{18} over 7 cells. Diffusion coefficients and fluorescence lifetimes were normalized to the mean pre-shear values (60 s for 20-s time steps and 30 s for 5-s time steps) for each cell independently. Significance tests were performed by computing two sample paired *t*-tests with respect to the pre-shear value immediately preceding step-shear (at 100 s for 20-s time steps and 115 s for 5-s time steps).

Shear Stress Induces Early and Transient Decrease in DiI-C_{12} Lifetime and Later and Sustained Decrease in DiI-C_{18} Lifetime

Fluorescence lifetime data were reported for 20-s integration time steps and plotted pre-, during and post-shear. DiI-C_{12} and DiI-C_{18} dyes exhibited double exponential lifetime (Fig. 2). From our solution results, model membrane results and literature,[55] we concluded that second lifetime component was more strongly affected by viscosity than the first component. Thus, we focused on the shear-induced changes in the longer exponent, for which values were obtained by tail fitting the portion of the histogram bin where first exponential and IRF are not relevant, i.e. 0.5 ns from maximum intensity.[7] The mean pre-shear lifetime values were $\tau_2 = 1.26 \pm 0.02$ ns for DiI-C_{12} and $\tau_2 = 1.43 \pm 0.05$ ns for DiI-C_{18}. From the data in Fig. 2 it is evident that shear stress induces a significant decrease in DiI-C_{12} normalized lifetime ($p < 0.05$) at 20 s after onset of shear whereas DiI-C_{18} exhibited a significant decrease in normalized lifetime beginning at 40 s ($p < 0.01$), which was sustained up until 120 s ($p < 0.01$) after onset of shear.

Lifetime data are also presented for 5-s time increments from 30 s before to 60 s after onset of shear. The mean values and standard errors for each dye are displayed in Fig. 3 for each time step. There was a significant decrease in the fluorescence lifetime for DiI-C_{12} cells that began at 10 s after step-shear and returned to control values after 35 s. DiI-C_{18} fluorescence lifetime, however, decreased beginning at 15 s after step-shear and this decrease was sustained for 55 s as shear continued. The points not showing significant changes in these intervals are likely due to natural membrane fluctuations in composition and viscosity. We conclude that shear stress induced a transient decrease in DiI-C_{12} lifetime with a characteristic time of 10 s, while the decrease with shear stress of DiI-C_{18} lifetime was delayed and sustained (Fig. 3).

Shear Stress Induces a Rapid Increase in Number of Molecules for DiI-C_{12} Domains and a Decrease for DiI-C_{18} Domains

For 5-s integration time, the normalized number of molecules (*N*) in the observation volume of DiI-C_{12} increased immediately and significantly after step shear and this increase was maintained for 15 s (Fig. 4). After 15 s *N* for DiI-C_{12} returned to pre-shear values despite the maintenance of shear stress. For DiI-C_{18}, *N* decreased immediately after step-shear but this decrease was transient.

Shear Stress Induced an Increase in Lateral Diffusion of DiI-C_{18} But Not DiI-C_{12}

Autocorrelation curves from fluorescence correlation spectroscopy measurements were derived from 20-s integration of step-shear data (Fig. 5). They were fit for 2-component 2-D diffusion,[60,75] where the fast component diffusion coefficient was in the range of that of free dye. The mean values of the slow components, corresponding to membrane diffusion, were $D_2 = 8.23 \pm 0.66 \times 10^{-8}$ cm^2/s (ranging from 6.34 to 10.4×10^{-8} cm^2/s) for DiI-C_{12} and $D_2 = 5.38 \pm 0.81 \times 10^{-8}$ cm^2/s (ranging from 1.77 to 10.1×10^{-8} cm^2/s) for DiI-C_{18}. Mean values and standard errors for normalized diffusion coefficients of the slow component are plotted over the time course of the experiment. We observed a significant increase ($p < 0.05$) in the diffusion coefficient of DiI-C_{18} between 20 and 40 s after onset of shear. There was no significant increase in diffusion of DiI-C_{12} for any time point.

DISCUSSION

To elucidate the role of the plasma membrane in endothelial cell sensitivity to shear stress, we recorded the change upon onset of shear in physical properties of fluorescent probes embedded in the lipid bilayer. Principle results are as follows. First, the chain lengths of DiI determine the domain phase specificity but are not related to chromophore photophysics. This result demonstrates that the differences in photophysical properties arise from differences in the local lipid bilayer the dyes are probing. Second, based on control data from GUVs and glycerol solutions of varying viscosity, a decrease in lifetime indicates a decrease in local molecular viscosity. Third, shear stress induces an early and transient decrease in DiI-C_{12} lifetime and a later sustained decrease in DiI-C_{18} lifetime. These decreases in lifetime can be attributed to shear-induced decreases in l_d and l_o membrane microviscosity around the DiI chromophore. Fourth, shear stress induces a rapid increase in number of molecules for DiI-C_{12} domains and a decrease for DiI-C_{18} domains, suggesting that the area of the membrane probed by DiI-C_{12} and DiI-C_{18} increases and decreases, respectively. Fifth, shear stress induced a later and transient increase in lateral diffusion of DiI-C_{18} but not DiI-C_{12}, suggesting that DiI-C_{18}-labeled domains become smaller and more mobile as a result of shear stress.

Our control studies on GUVs show that the shorter lifetime and faster diffusion of DiI-C_{12} relative to DiI-C_{18} in cells is due to the fact that the DiI chromophore responds to local differences in lipid phase. Diffusion coefficients of DiI-C_{12} and DiI-C_{18} collected in giant unilamellar vesicles were consistent with those found in other studies[1,38] and illustrate that both dyes diffuse similarly in similar lipid phases (Table 1).Mean diffusion coefficients in cells show that the dyes in the plasma membrane probe two different domains: DiI-C_{12} is in a l_d environment, while DiI-C_{18} probes l_o domains. We can also conclude that the main non-radiative pathway for DiI is through trans-cis photoisomerization of the chromophore's central methine bridge and this pathway is augmented when viscosity surrounding the chormophore decreases. In previous research we have found that the DiI chromophores are located within the lipid bilayer just below the lipid headgroups[33] and we did not detect large effects from increasing water accessibility on lifetime values (Fig. 1b). We also assume uniformity of electrostatic charge fields around the bilayer and sufficiently low dye

concentration such that homo-FRET is prevented. Importantly, an increase in lifetime with increasing glycerol concentrations (Fig. 1a) points to local viscosity as the main cause of lifetime changes. Accordingly, since average lifetime values obtained from shear experiments were consistently higher than in our GUV and solution controls we conclude that cells have more viscous membranes than model membranes. Combining control data with shear data, and since DiI labels the outer leaflet of cells, we conclude that our reported decreases in fluorescence lifetime with shear stress reflect decreases in viscosity of the outer leaflet of the cell membrane that are early and transient for l_d domains and later and sustained for l_o domains.

As mentioned in methods, the effects of shear stress on membrane microdomains were evaluated at a single point on the apical endothelial cell membrane at a position upstream from the nucleus. Because data was recorded continuously on a single point per cell, in order to record time-dependent events, it was not possible to scan multiple points on the cell. The upstream side of the cell was chosen because previous research showed that shear effects on membranes were most prominent in this area.[10] Recent studies by Dangaria *et al*.[15] and Ueki *et al*.[73] suggest that the upstream part of the apical cell surface experiences greater strain than other parts of the cell surface in response to fluid shear stress. Related to his, Barbee *et al*. have suggested that this area of the cell experiences positive spatial shear stress gradients, in contrast to the downstream side, where spatial shear stress gradients are negative.[5] Our previous research also suggests that the upstream side of the cell is differentially sensitive to temporal shear stress gradients and these effects are rapidly attenuated after step shear, and absent during ramp and steady shear.[11] For these reasons, we evaluated step shear effects, containing both temporal shear gradients and steady shear components, on the upstream side of the cell, where shear stress is higher and there exists positive shear stress gradients. Considering this heterogeneity of stress distributions, we expect that shear effects on membrane microdomains on other parts of the cell are also spatially varying. In addition heterogeneity in stress in a membrane of heterogonous composition may contribute to spatially varying effects of shear stress observed during calcium signaling,[30] stretch on membrane ruffling,[36] and shear on mechanotaxis,[47] and other shear related phenomenon. In our studies, cells were confluent. Confluent cells are likely to have different stress distributions than non-confluent cells. Thus, confluence is another factor that could potentially contribute to stress heterogeneity.[72] Finally, we have looked at detailed stress distributions in focal adhesions[24] and have predicted that these are areas with additional stress heterogeneity. Thus the detailed role of stress heterogeneity on cell membrane sensitivity to shear stress remains a fruitful avenue of future research.

Synthesis of all the data obtained from multiparameter TCSPC leads us to suggest that shear stress rapidly and transiently induces membrane rippling of the liquid-disordered domains leading to decreased viscosity in the outer leaflet. Support for this interpretation is as follows. The number of DiI-C_{12} molecules increased by about 30% immediately after onset of shear (Fig. 4). This phenomenon did not result from a change of focus or membrane angle since there was no decrease in molecular brightness (data not shown) or decrease in diffusion coefficient (Fig. 5).[50,65] Thus, the increase in *N* is only possible when the surface area of the membrane probed by the confocal volume increases. A possible explanation is shear-induced membrane ripples which may be caused by force transmission from the flow to the glycocalyx to the membrane. In fact, the role of the glycocalyx has been purported to impair fluid flow near the lipid bilayer[14,61] and may, itself, act as a mechanosensor.[69,76] Although there is still controversy about its integrity in cultured cells,[58] immunofluorescence of heparin sulfate proteoglycans show that it is at least present in cultured endothelial cells used in our experiments (Fig. 6).[25,74] A documented pattern for the glycocalyx has displayed syndecan-actin cytoskeleton anchors 100 nm apart[67] and a mechanism for translation of the mechanical stress from fluid flow to the cell has been

described by a moment about an axis normal to the direction of shear on anchored syndecans.[76] If undulations occurred between anchored points, the surface area between each could increase by about 30%. Assuming a sinusoidal wave, the membrane undulation would have an 18-nm amplitude.[50] Undulations that increase the surface area by 30% should decrease the apparent diffusion coefficient of the dye by approximately the same amount. Either FCS measurements were not sufficiently sensitive to detect this change, or the lateral mobility of the dye was also enhanced by shear and cancelled out the undulation effect. The decrease in lifetime of DiI-C_{12} at shortly after step-shear (Fig. 3), reflecting a decrease in viscosity, is consistent with this interpretation. Since the dye resides in the outer leaflet during the experimental time, the recorded viscosity decrease might come from outward membrane bending resulting in tension in the outer leaflet and reduced lipid order. GPI-anchored proteoglycans, glypicans, float on the upper leaflet and can also translate mechanical force through lateral motion. In summary, the decrease in lifetime for DiI-C_{12} and increase in molecular number with shear stress is consistent with a decrease in viscosity of the outer membrane leaflet resulting from outward curvature and the associated expansion of the outer membrane leaflet. Assessing the role of the glycocalyx in shear-induced membrane rippling would be an interesting avenue of investigation, but care would need to be exercised because of the subtle influence on bilayer organization of extracellular and intracellular structural components, as demonstrated in changes in fluorescence lifetime of dyes when cells were incubated with and without serum. For these reasons, repeating these experiments with the glycocalyx removed was beyond the scope of this study.

An alternative interpretation to the change in *N* is that shear stress simply strained the membrane and increased its area. If this were the case then *N* would decrease since the confocal probe cross-sectional area does not change. *N* did decrease transiently for DiI-C_{18} but increased for DiI-C_{12}, So simple strain is not sufficient to explain the differential effects of shear on *N*. It is also possible, that because the membrane is fluid, stress caused DiI-C_{18} molecules to leave the probe area while it caused DiI-C_{12} molecules to enter. A possible mechanism of this might be stress-induced thinning of the membrane resulting in changes in the probes' preference for the location that was being monitored. This is an entirely plausible explanation since the miscibility of the dyes in the membrane depends strongly on chain length matching between DiI and the local bilayer. Thinning the bilayer would favor miscibility of DiI-C_{12} and disfavor miscibility of DiI-C_{18} leading to lateral diffusion toward or away from, respectively, the observation area. This hypothesis leads to the interesting idea that shear stress leads to lipid sorting through hydrophobic interactions among lipids. A similar effect could apply to proteins which much match their hydrophobic regions to lipid hydrophobic regions.

The wider range of diffusion coefficient values of DiI-C_{18} reflects the heterogeneous nature of the domains it resides in—DiI-C_{18} has been localized in higher-order lipid domains[16] as well as in less packed high-ordered lipid domains,[48] and GPI-anchored proteins, thought to co-localize with liquid-ordered domains, can display relatively fast lateral diffusion.[39] Regarding the effects of shear on l_o domains, we recorded a delayed and transient increase in DiI-C_{18} diffusion coefficient after shear (Fig. 5). Simultaneously, we showed that fluorescence lifetime values decreased 10 s after onset of shear (Fig. 3), but remained low as long as shear was on (Fig. 2). Together, these data indicate that shear stress reduced viscosity of liquid-ordered (l_o) domains. Again, from data recorded simultaneously for diffusion and lifetime, we proposed that shear-induced increase in l_o domain diffusion are are due to changes in the size of the domains probed by DiI-C_{18}, decreased viscosity of membrane surrounding l_o membrane, or shear-induced increase in lateral diffusion of GPI-anchored proteins.[39]

In summary, the shear-induced decrease in fluorescence lifetime of DiI-C_{12} can be explained by shear-induced undulations and local decrease in outer leaflet viscosity of l_d phase domains. This could be due to the twisting of the lipid bilayer from the moment (torque) transmitted from the fluid flow to syndecans and glypicans. The increase in diffusion coefficient of DiI-C_{18} recorded by FCS may be caused by the decreased size of domains, increased mobility of the surrounding fluid phase, or drag by glypicans. Also, the sustained decrease in lifetime of DiI-C_{18} during application of the fluid shear stress may result from constant mechanical strain felt locally. Alternatively, shear stress leads to membrane thinning resulting in changes in preference for the dyes in the observation area, changes in their fluorescence lifetime, and diffusion coefficients. It should be pointed out, however, that several signaling events are triggered within the course of this experiment. G proteins and ion channels, in particular, are activated within seconds[13,31,53] and could be the cause of the stress regulation or cross-linking of proteins, which may affect local membrane viscosity. Lipid turnover, as well, can occur within seconds, as seen in neuronal cells. But from the perspective of a passive response, stress could be transferred from fluid phase to ordered domains within seconds. The time-line of shear effects for DiI-C_{12} (early) and DiI-C_{18} (later) are consistent with the interpretation that the short term responses of the membrane to shear stress reflect a passive response.

In conclusion, this study revealed time-dependent changes in membrane microviscosity using simultaneous fluorescence correlation spectroscopy, fluorescence lifetime, and molecular brightness measurements of lipoid dyes embedded in endothelial cell membranes. This novel multiparameter approach to single-molecule spectroscopy to study membrane dynamics allowed us to gain insight into the temporal, spatial, and domain-dependent alteration of the endothelial cell lipid bilayer in response to physiological shear stress.

Acknowledgments

This work was supported by grants to PJB from the National Heart Lung and Blood Institute (R01 HL 07754201-A1) and the National Science Foundation (BES 0238910).

REFERENCES

1. Almeida PF, Vaz WL, Thompson TE. Lateral diffusion in the liquid phases of dimyristoylphosphatidylcholine/cholesterol lipid bilayers: a free volume analysis. Biochemistry. 1992; 31:6739–6747. [PubMed: 1637810]
2. Anderson RG, Jacobson K. A role for lipid shells in targeting proteins to caveolae, rafts, and other lipid domains. Science. 2002; 296:1821–1825. [PubMed: 12052946]
3. Bacia K, Scherfeld D, Kahya N, Schwille P. Fluorescence correlation spectroscopy relates rafts in model and native membranes. Biophys. J. 2004; 87:1034–1043. [PubMed: 15298908]
4. Bao X, Clark CB, Frangos JA. Temporal gradient in shear-induced signaling pathway: involvement of MAP kinase, c-fos, and connexin43. Am. J. Physiol. Heart Circ. Physiol. 2000; 278:H1598–H1605. [PubMed: 10775139]
5. Barbee KA. Role of subcellular shear-stress distributions in endothelial cell mechanotransduction. Ann. Biomed. Eng. 2002; 30:472–482. [PubMed: 12085999]
6. Becker W, Bergmann A, Haustein E, Petrasek Z, Schwille P, Biskup C, Kelbauskas L, Benndorf K, Klocker N, Anhut T, Riemann I, Konig K. Fluorescence lifetime images and correlation spectra obtained by multidimensional time-correlated single photon counting. Microsc. Res. Tech. 2006; 69:186–195. [PubMed: 16538624]
7. Benda A, Fagul'ova V, Deyneka A, Enderlein J, Hof M. Fluorescence lifetime correlation spectroscopy combined with lifetime tuning: new perspectives in supported phospholipid bilayer research. Langmuir. 2006; 22:9580–9585. [PubMed: 17073482]

8. Brown DA, London E. Structure of detergent-resistant membrane domains: does phase separation occur in biological membranes? Biochem. Biophys. Res. Commun. 1997; 240:1–7. [PubMed: 9367871]
9. Brown DA, Rose JK. Sorting of GPI-anchored proteins to glycolipid-enriched membrane subdomains during transport to the apical cell surface. Cell. 1992; 68:533–544. [PubMed: 1531449]
10. Butler PJ, Norwich G, Weinbaum S, Chien S. Shear stress induces a time- and position-dependent increase in endothelial cell membrane fluidity. Am. J. Physiol. Cell Physiol. 2001; 280:C962–C969. [PubMed: 11245613]
11. Butler PJ, Tsou TC, Li JY, Usami S, Chien S. Rate sensitivity of shear-induced changes in the lateral diffusion of endothelial cell membrane lipids: a role for membrane perturbation in shear-induced MAPK activation. FASEB J. 2002; 16:216–218. [PubMed: 11744620]
12. Chachisvilis M, Zhang YL, Frangos JA. G protein-coupled receptors sense fluid shear stress in endothelial cells. Proc. Natl. Acad. Sci. USA. 2006; 103:15463–15468. [PubMed: 17030791]
13. Cooke JP, Rossitch E Jr, Andon NA, Loscalzo J, Dzau VJ. Flow activates an endothelial potassium channel to release an endogenous nitrovasodilator. J. Clin. Invest. 1991; 88:1663–1671. [PubMed: 1719029]
14. Damiano ER, Long DS, Smith ML. Estimation of viscosity profiles using velocimetry data from parallel flows of linearly viscous fluids: application to microvascular haemodynamics. J. Fluid Mech. 2004; 512:1–19.
15. Dangaria JH, Butler PJ. Macrorheology and adaptive microrheology of endothelial cells subjected to fluid shear stress. Am. J. Physiol. Cell Physiol. 2007; 293:C1568–C1575. [PubMed: 17670893]
16. Davey AM, Walvick RP, Liu YX, Heikal AA, Sheets ED. Membrane order and molecular dynamics associated with IgE receptor cross-linking in mast cells. Biophys. J. 2007; 92:343–355. [PubMed: 17040981]
17. Davies PF. Flow-mediated endothelial mechanotransduction. Physiol. Rev. 1995; 75:519–560. [PubMed: 7624393]
18. Davies PF. Overview: temporal and spatial relationships in shear stress-mediated endothelial signalling. J. Vasc. Res. 1997; 34:208–211. [PubMed: 9226302]
19. dePaola N, Gimbrone MA Jr, Davies PF, Dewey CF Jr. Vascular endothelium responds to fluid shear stress gradients. Arterioscler. Thromb. 1992; 12:1254–1257. [PubMed: 1420084]
20. Dimitrov DS, Angelova MI. Electric-field mediated lipid swelling and liposome formation. Studia Biophysica. 1987; 119:61–65.
21. Duncan RR, Bergmann A, Cousin MA, Apps DK, Shipston MJ. Multi-dimensional time-correlated single photon counting (TCSPC) fluorescence lifetime imaging microscopy (FLIM) to detect FRET in cells. J. Microsc.-Oxford. 2004; 215:1–12.
22. Elson EL, Magde D. Fluorescence correlation spectroscopy. 1. Conceptual basis and theory. Biopolymers. 1974; 13:1–27.
23. Ferko MC, Patterson BP, Butler PJ. High-resolution solid modeling of biological samples imaged with 3D fluorescence microscopy. Mic. Res. Tech. 2006; 69(8):648–655.
24. Ferko MC, Bhatnagar A, Garcia MB, Butler PJ. Finite-element stress analysis of a multicomponent model of sheared and focally-adhered endothelial cells. Ann. Biomed. Eng. 2007; 35:208–223. [PubMed: 17160699]
25. Florian JA, Kosky JR, Ainslie K, Pang Z, Dull RO, Tarbell JM. Heparan sulfate proteoglycan is a mechanosensor on endothelial cells. Circ. Res. 2003; 93:e136–e142. [PubMed: 14563712]
26. Frangos JA, Huang TY, Clark CB. Steady shear and step changes in shear stimulate endothelium via independent mechanisms—superposition of transient and sustained nitric oxide production. Biochem. Biophys. Res. Commun. 1996; 224:660–665. [PubMed: 8713104]
27. Fujiwara K, Masuda M, Osawa M, Kano Y, Katoh K. Is PECAM-1 a mechanoresponsive molecule? Cell Struct. Funct. 2001; 26:11–17. [PubMed: 11345499]
28. Galbraith CG, Skalak R, Chien S. Shear stress induces spatial reorganization of the endothelial cell cytoskeleton. Cell Motil. Cytoskeleton. 1998; 40:317–330. [PubMed: 9712262]
29. Girard PR, Nerem RM. Endothelial cell signaling and cytoskeletal changes in response to shear stress. Front Med. Biol. Eng. 1993; 5:31–36. [PubMed: 8323880]

30. Goligorsky MS. Mechanical stimulation induces Ca2+i transients and membrane depolarization in cultured endothelial cells. Effects on Ca2+i in co-perfused smooth muscle cells. FEBS Lett. 1988; 240:59–64. [PubMed: 3192000]

31. Gudi SR, Clark CB, Frangos JA. Fluid flow rapidly activates G proteins in human endothelial cells. Involvement of G proteins in mechanochemical signal transduction. Circ. Res. 1996; 79:834–839. [PubMed: 8831508]

32. Gullapalli RR, Tabouillot T, Mathura R, Dangaria JH, Butler PJ. Integrated multimodal microscopy, time-resolved fluorescence, and optical-trap rheometry: toward single molecule mechanobiology. J. Biomed. Opt. 2007; 12 014012.

33. Gullapalli RR, Demirel MC, Butler PJ. Molecular dynamics simulations of DiI-C18(3) in a DPPC lipid bilayer. Phys. Chem. Chem. Phys. 2008; 10:3548–3560. [PubMed: 18548161]

34. Hao M, Mukherjee S, Maxfield FR. Cholesterol depletion induces large scale domain segregation in living cell membranes. Proc. Natl. Acad. Sci. USA. 2001; 98:13072–13077. [PubMed: 11698680]

35. Hess ST, Webb WW. Focal volume optics and experimental artifacts in confocal fluorescence correlation spectroscopy. Biophys. J. 2002; 83:2300–2317. [PubMed: 12324447]

36. Huang L, Mathieu PS, Helmke BP. A stretching device for high-resolution live-cell imaging. Ann. Biomed. Eng. 2010; 38:1728–1740. [PubMed: 20195762]

37. Jacobs ER, Cheliakine C, Gebremedhin D, Birks EK, Davies PF, Harder DR. Shear activated channels in cell-attached patches of cultured bovine aortic endothelial cells. Pflugers Arch. 1995; 431:129–131. [PubMed: 8584410]

38. Kahya N, Scherfeld D, Bacia K, Schwille P. Lipid domain formation and dynamics in giant unilamellar vesicles explored by fluorescence correlation spectroscopy. J. Struct. Biol. 2004; 147:77–89. [PubMed: 15109608]

39. Kenworthy AK, Nichols BJ, Remmert CL, Hendrix GM, Kumar M, Zimmerberg J, Lippincott-Schwartz J. Dynamics of putative raft-associated proteins at the cell surface. J. Cell Biol. 2004; 165:735–746. [PubMed: 15173190]

40. Klausner RD, Wolf DE. Selectivity of fluorescent lipid analogues for lipid domains. Biochemistry. 1980; 19:6199–6203. [PubMed: 7470460]

41. Korlach J, Schwille P, Webb WW, Feigenson GW. Characterization of lipid bilayer phases by confocal microscopy and fluorescence correlation spectroscopy. Proc. Natl. Acad. Sci. USA. 1999; 96:8461–8466. [PubMed: 10411897]

42. Kusumi A, Suzuki K. Toward understanding the dynamics of membrane-raft-based molecular interactions. Biochim. Biophys. Acta. 2005; 1746:234–251. [PubMed: 16368465]

43. Lakowicz, JR. Principles of Fluorescence Spectroscopy. Springer; 1999.

44. LaMack JA, Friedman MH. Individual and combined effects of shear stress magnitude and spatial gradient on endothelial cell gene expression. Am. J. Physiol. Heart Circ. Physiol. 2007; 293:H2853–H2859. [PubMed: 17766484]

45. Levitan I, Christian AE, Tulenko TN, Rothblat GH. Membrane cholesterol content modulates activation of volume-regulated anion current in bovine endothelial cells. J. Gen. Physiol. 2000; 115:405–416. [PubMed: 10736308]

46. Li S, Kim M, Hu YL, Jalali S, Schlaepfer DD, Hunter T, Chien S, Shyy JY. Fluid shear stress activation of focal adhesion kinase. Linking to mitogen-activated protein kinases. J. Biol. Chem. 1997; 272:30455–30462. [PubMed: 9374537]

47. Li S, Butler P, Wang YX, Hu YL, Han DC, Usami S, Guan JL, Chien S. The role of the dynamics of focal adhesion kinase in the mechanotaxis of endothelial cells. Proc. Natl. Acad. Sci. USA. 2002; 99:3546–3551. [PubMed: 11891289]

48. Loura LM, Fedorov A, Prieto M. Partition of membrane probes in a gel/fluid two-component lipid system: a fluorescence resonance energy transfer study. Biochim. Biophys. Acta. 2000; 1467:101–112. [PubMed: 10930513]

49. Magde D, Elson EL, Webb WW. Fluorescence correlation spectroscopy. 2. Experimental realization. Biopolymers. 1974; 13:29–61. [PubMed: 4818131]

50. Milon S, Hovius R, Vogel H, Wohland T. Factors influencing fluorescence correlation spectroscopy measurements on membranes: simulations and experiments. Chem. Phys. 2003; 288:171–186.
51. Mochizuki S, Vink H, Hiramatsu O, Kajita T, Shigeto F, Spaan JA, Kajiya F. Role of hyaluronic acid glycosaminoglycans in shear-induced endothelium-derived nitric oxide release. Am. J. Physiol. Heart Circ. Physiol. 2003; 285:H722–H726. [PubMed: 12730059]
52. Ohno M, Gibbons GH, Dzau VJ, Cooke JP. Shear stress elevates endothelial cGMP. Role of a potassium channel and G protein coupling. Circulation. 1993; 88:193–197. [PubMed: 8391400]
53. Olesen SP, Clapham DE, Davies PF. Haemodynamic shear stress activates a K+ current in vascular endothelial cells. Nature. 1988; 331:168–170. [PubMed: 2448637]
54. Orr AW, Helmke BP, Blackman BR, Schwartz MA. Mechanisms of mechanotransduction. Dev. Cell. 2006; 10:11–20. [PubMed: 16399074]
55. Packard BS, Wolf DE. Fluorescence lifetimes of carbocyanine lipid analogues in phospholipid bilayers. Biochemistry. 1985; 24:5176–5181. [PubMed: 4074686]
56. Pahakis MY, Kosky JR, Dull RO, Tarbell JM. The role of endothelial glycocalyx components in mechanotransduction of fluid shear stress. Biochem. Biophys. Res. Commun. 2007; 355:228–233. [PubMed: 17291452]
57. Park H, Go YM, Darji R, Choi JW, Lisanti MP, Maland MC, Jo H. Caveolin-1 regulates shear stress-dependent activation of extracellular signal-regulated kinase. Am. J. Physiol. Heart Circ. Physiol. 2000; 278:H1285–H1293. [PubMed: 10749726]
58. Potter DR, Damiano ER. The hydrodynamically relevant endothelial cell glycocalyx observed in vivo is absent in vitro. Circ. Res. 2008; 102:770–776. [PubMed: 18258858]
59. Rizzo V, Sung A, Oh P, Schnitzer JE. Rapid mechanotransduction in situ at the luminal cell surface of vascular endothelium and its caveolae. J. Biol. Chem. 1998; 273:26323–26329. [PubMed: 9756862]
60. Schwille P, Korlach J, Webb WW. Fluorescence correlation spectroscopy with single-molecule sensitivity on cell and model membranes. Cytometry. 1999; 36:176–182. [PubMed: 10404965]
61. Secomb TW, Hsu R, Pries AR. Effect of the endothelial surface layer on transmission of fluid shear stress to endothelial cells. Biorheology. 2001; 38:143–150. [PubMed: 11381171]
62. Seong J, Lu S, Ouyang M, Huang H, Zhang J, Frame MC, Wang Y. Visualization of Src activity at different compartments of the plasma membrane by FRET imaging. Chem. Biol. 2009; 16:48–57. [PubMed: 19171305]
63. Sheets ED, Lee GM, Simson R, Jacobson K. Transient confinement of a glycosylphosphatidylinositol-anchored protein in the plasma membrane. Biochemistry. 1997; 36:12449–12458. [PubMed: 9376349]
64. Sigurdson WJ, Sachs F, Diamond SL. Mechanical perturbation of cultured human endothelial cells causes rapid increases of intracellular calcium. Am. J. Physiol. 1993; 264:H1745–H1752. [PubMed: 8322903]
65. Sorscher SM, Klein MP. Profile of a focused collimated laser-beam near the focal minimum characterized by fluorescence correlation spectroscopy. Rev. Sci. Instrum. 1980; 51:98–102.
66. Spink CH, Yeager MD, Feigenson GW. Partitioning behavior of indocarbocyanine probes between coexisting gel and fluid phases in model membranes. Biochim. Biophys. Acta. 1990; 1023:25–33. [PubMed: 2317494]
67. Squire JM, Chew M, Nneji G, Neal C, Barry J, Michel C. Quasi-periodic substructure in the microvessel endothelial glycocalyx: a possible explanation for molecular filtering? J. Struct. Biol. 2001; 136:239–255. [PubMed: 12051903]
68. Tabouillot, T.; Gullapalli, RR.; Butler, PJ. Monitoring cellular mechanosensing using time-correlated single photon counting; Proc.SPIE; 2006. p. 63720DRef Type: Conference Proceeding
69. Tarbell JM, Pahakis MY. Mechanotransduction and the glycocalyx. J. Intern. Med. 2006; 259:339–350. [PubMed: 16594902]
70. Thi MM, Tarbell JM, Weinbaum S, Spray DC. The role of the glycocalyx in reorganization of the actin cytoskeleton under fluid shear stress: a “bumper-car” model. Proc. Natl. Acad. Sci. USA. 2004; 101:16483–16488. [PubMed: 15545600]

71. Tzima E. Role of small GTPases in endothelial cytoskeletal dynamics and the shear stress response. Circ. Res. 2006; 98:176–185. [PubMed: 16456110]

72. Ueki Y, Sakamoto N, Ohashi T, Sato M. Morphological responses of vascular endothelial cells induced by local stretch transmitted through intercellular junctions. Exp. Mech. 2009; 49:125–134.

73. Ueki Y, Sakamoto N, Sato M. Direct measurement of shear strain in adherent vascular endothelial cells exposed to fluid shear stress. Biochem. Biophys. Res. Commun. 2010; 394:94–99. [PubMed: 20175996]

74. Vijayagopal P, Srinivasan SR, Dalferes ER Jr, Radhakrishnamurthy B, Berenson GS. Effect of low-density lipoproteins on the synthesis and secretion of proteoglycans by human endothelial cells in culture. Biochem. J. 1988; 255:639–646. [PubMed: 3202837]

75. Wawrezinieck L, Rigneault H, Marguet D, Lenne PF. Fluorescence correlation spectroscopy diffusion laws to probe the submicron cell membrane organization. Biophys. J. 2005; 89:4029–4042. [PubMed: 16199500]

76. Weinbaum S, Zhang X, Han Y, Vink H, Cowin SC. Mechanotransduction and flow across the endothelial glycocalyx. Proc. Natl. Acad. Sci. USA. 2003; 100:7988–7995. [PubMed: 12810946]

77. Widengren J, Rigler R. Photobleaching investigations of dyes using fluorescence correlation spectroscopy (FCS). Prog. Biophys. Mol. Biol. 1996; 65:H109.

78. Widengren J, Mets U, Rigler R. Fluorescence correlation spectroscopy of triplet states in solution: a theoretical and experimental study. J. Phys. Chem. 1995; 99:13368–13379.

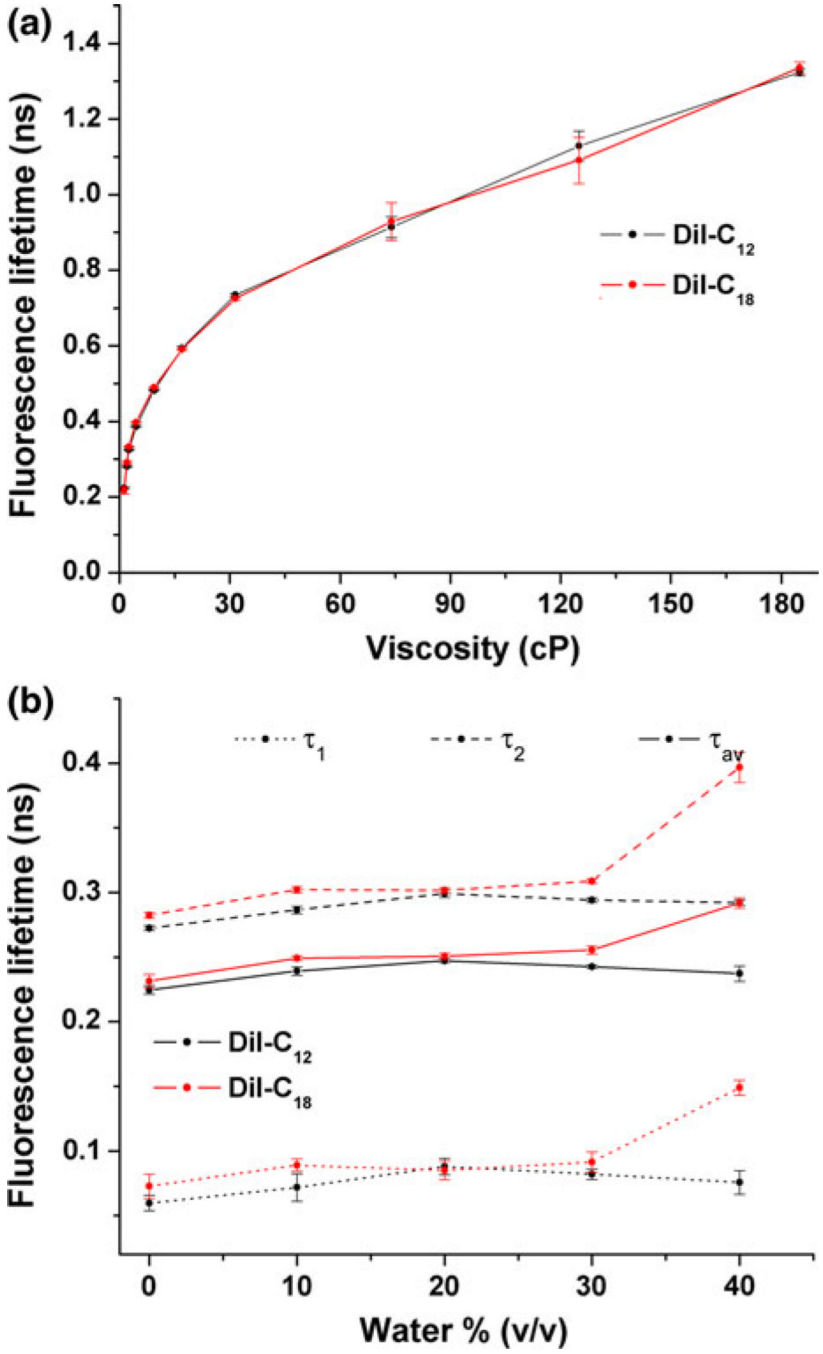

FIGURE 1.

Assessment of fluorescence lifetime decay mechanisms of DiI: (a) Effects of solution viscosity on fluorescence lifetime (means and standard deviations) of DiI-C_{12} and DiI-C_{18}. Viscosity was increased by increasing glycerol concentration and was measured in a viscometer. (b) Effect of increasing water content on fluorescence lifetime (means and standard deviations) of DiI-C_{12} and DiI-C_{18}.

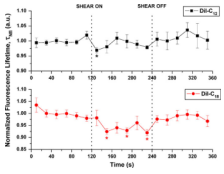

FIGURE 2.

Effect of shear stress on 20-s normalized fluorescence lifetime of membrane dyes DiI-C_{12} (n = 7) and DiI-C_{18} (n = 8). All lifetimes were evaluated using 20-s integration of photon data, tail fitted for the slow exponent only, were normalized using average of pre-shear values, and are expressed as means and standard errors. Vertical dotted line indicates shear on (or off) time point (*$p < 0.05$).

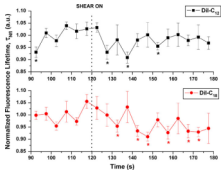

FIGURE 3.

Effect of shear stress on 5-s normalized fluorescence lifetime of membrane dyes DiI-C_{12} (n = 7) and DiI-C_{18} (n = 8). All lifetimes were evaluated using 5-s integration of photon data, tail fitted for the slow exponent only, were normalized using average of pre-shear values, and are expressed as means and standard errors. Vertical dotted line indicates shear on time point (*$p < 0.05$).

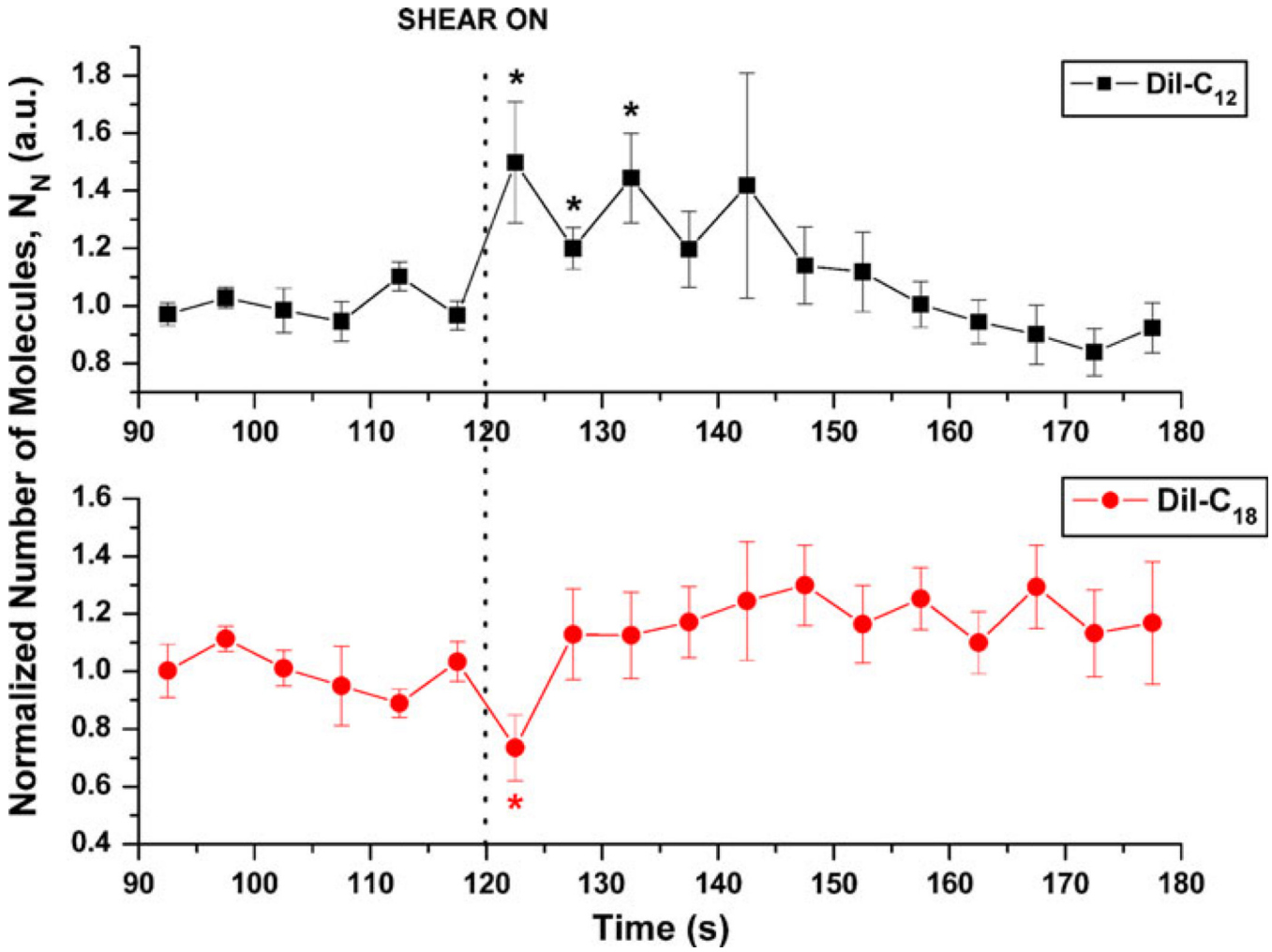

FIGURE 4.

Effects of shear stress on 5-s normalized number of molecules, *N*, relative to last pre-shear value for DiI-C_{12} (n = 7) and DiI-C_{18} (n = 8). Values are normalized to average of pre-shear values and expressed as means and standard errors. Vertical dotted line indicates shear on (or off) time point (* $p < 0.05$).

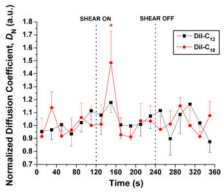

FIGURE 5.

Effects of shear stress on 20-s normalized diffusion coefficient, *D*, relative to last pre-shear value, for DiI-C_{12} (n = 7) and DiI-C_{18} (n = 8). All diffusion coefficients were evaluated using 20-s integration of photon data, were normalized using average of pre-shear values, and are expressed as means and standard errors. Vertical dotted line indicates shear on (or off) time point (* $p < 0.05$).

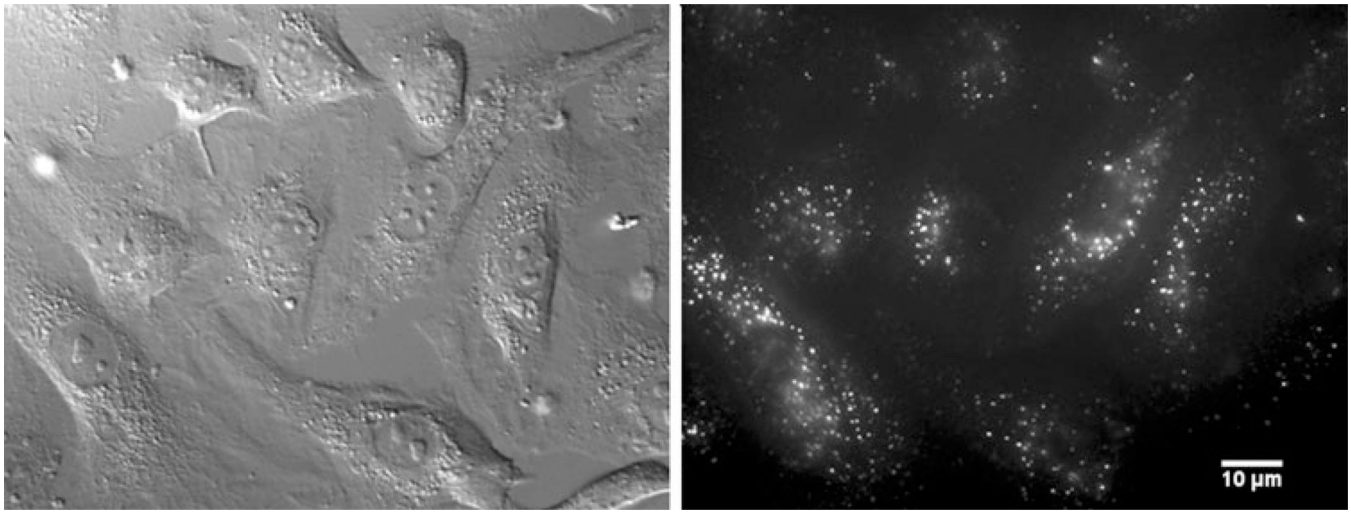

FIGURE 6.
Glycocalyx staining of BAECs with Alexa Fluor 647-tagged HepSS-1. Staining pattern is similar that reported in Thi.[70]

TABLE 1

Diffusion coefficients and lifetime values of DiI-C_{12} and DiI-C_{18}.

D **(×10^{-8} cm^2/s);** **τ_1 (ns),** **τ_2 (ns)**		
	DiI-C_{12}	**DiI-C_{18}**
DOPC (l_d)	8.2 ± 0.4; 0.29 ± 0.01, 0.92 ± 0.01	7.8 ± 0.5; 0.28 ± 0.02, 0.93 ± 0.02
DOPC:cholesterol (1:1) (l_o)	5.0 ± 0.2*; 0.36 ± 0.02, 1.07 ± 0.02*	5.0 ± 0.2*; 0.36 ± 0.02, 1.08 ± 0.01*
DPPC (gel)	Immobile; 0.34 ± 0.03, 1.28 ± 0.04*	Immobile; 0.29 ± 0.05, 1.31 ± 0.02*
BAECs in DPBS	NA; NA, 1.09 ± 0.08	NA; NA, 1.12 ± 0.08**
BAECs in DPBS with MβCD	NA; NA, 1.07 ± 0.04	NA; NA, 1.04 ± 0.06**,***
BAECs in DMEM + FBS	8.23 ± 0.66; NA, 1.26 ± 0.02†	5.38 ± 0.81; NA, 1.43 ± 0.05**,†

Rows 1–3 are diffusion coefficients and lifetime values (±SD) of DiI-C_{12} and DiI-C_{18} in giant unilamellar vesicles in l_d (DOPC), l_o (DOPC:cholesterol in a 1:1 mol fraction) and gel (DPPC) phases.

* Indicates significant differences between each phase for diffusion and τ_2 (n = 10) ($p < 0.05$). Rows 4–5 are tail-fitted lifetime values (±SD) of DiI-C_{12} and DiI-C_{18} in bovine aortic endothelial cells (BAECs) in DPBS (n = 11).

** indicates significant difference between lifetime values for DiI-C_{12} (n = 10) and DiI-C_{18} (n = 12).

*** indicates significant difference in lifetime values for BAECs in DPBS and DPBS with MβCD (in these experiments D was not measured and τ_1 is not relevant for tail fitting). Row 6 is diffusion coefficient and tail-fitted lifetime values in cells in DMEM with FBS.

† indicates significant difference of diffusion or lifetime values for cells in serum vs. DPBS without serum).